Tool Wear Prediction Using a Hybrid of Tool Chip Image and Evolutionary Fuzzy Neural Network

Cheng-Jian Lin (cjlin@ncut.edu.tw)
National Chin-Yi University of Technology
Jyun-Yu Jhang
National Chin-Yi University of Technology
Shao-Hsien Chen
National Chin-Yi University of Technology

Research Article

Keywords: tool wear, chip surface, color calibration, evolutionary fuzzy neural network, particle swarm optimization

Posted Date: March 15th, 2021

DOI: https://doi.org/10.21203/rs.3.rs-177548/v1

Version of Record: A version of this preprint was published at The International Journal of Advanced Manufacturing Technology on September 10th, 2021. See the published version at https://doi.org/10.1007/s00170-021-07291-0.

Tool Wear Prediction Using a Hybrid of Tool Chip Image and Evolutionary Fuzzy Neural Network

Cheng-Jian Lin[1, 2*], Jyun-Yu Jhang[1,2], Shao-Hsien Chen[4]

[1]Department of Computer Science and Information Engineering, National Chin-Yi University of Technology, Taichung 411, Taiwan

[2]College of Intelligence, National Taichung University of Science and Technology, Taichung 404, Taiwan

[3]Department of Mechanical Engineering, National Chin-Yi University of Technology, Taichung 411, Taiwan

(*corresponding author; Email: cjlin@ncut.edu.tw)

Abstract

This paper proposed an evolutionary fuzzy neural network (EFNN) for tool wear prediction. The material chip is affected by cutting conditions during the cutting process. The different tool wear status causes different chip color which means the color of material chip can be an important factor for tool wear prediction. In this study, an industrial camera is used to capture chip image and convert it into CIE *xy* chromaticity features through a color conversion model. In addition, to improve the prediction accuracy, a dynamic group cooperative particle swarm optimization (DGCPSO) is proposed to optimize the EFNN parameters. The cutting time and CIE *xy* value are used as the input of the EFNN, and the output is predicted tool wear value. The experimental results show that the mean absolute percentage error (MAPE) of the proposed EFNN is 2.83% better than other methods.

Keywords: tool wear, chip surface, color calibration, evolutionary fuzzy neural network, particle swarm optimization

I. Introduction

Tool life prediction is one of the most important technologies in the machinery industry. When tool wear occurs, it affects the accuracy of the product, resulting in an increase defect rate of the product and cost. Many researchers have studied the field of tool wear prediction in order to improve the accuracy of prediction [1-2]. The researches on tool wear are extensive such as process parameters, down milling, up milling, cutting force measurement, and sensor signals from machine [3-4]. The approach using signals acquired by sensors is an indirect way that is difficult to reflect the actual cutting situation [5-6]. On the other hand, the measurement of the sensor needs to pass the force flow line. Using the sensor to measure tools of different materials will obtain different signal values. In this way, the established tool wear prediction model is only for one type of tool. Instead of using sensor signals, the chip is directly affected by the cutting force, shape of tool and the heat during the cutting process [7-8]. During the cutting process, the chip tool will directly contact the tool that is more reflective of the current situation of cutting than the method of measuring signals by sensors. Thus, this paper adopts the chip surface color as feature value which is able to correspond to the temperature of cutting procedure as well as reflect the current cutting status to further enhance the

accuracy of tool wear prediction.

In tool wear prediction, neural network (NN) has been widely used in the establishment of prediction model [9]. The advantages of NN are simple structure, training fast, and does not need to design complicated mathematical models. The behavior of the network tends to exhibit a black-box that does not explain in a way that humans can understand. The fuzzy neural network (FNN) which combines fuzzy logic and NN has been proposed for various applications [10]. Different from NN, the fuzzy logic applied by FNN is realized in spirit to human reasoning and natural language expression [11-13]. The fuzzy logic adopts linguistic information to model the reasoning processes with qualitative aspects of human knowledge without utilizing precise quantitative analyzes [14-15]. Therefore, fuzzy logic is closer to human experience and practice in the description and interpretation of information. Through introducing the concept of membership degree, FNN has the abilities to deal with inaccuracy and uncertainty problems [16-17]. Chungchoo and Saini [18] proposed a new on-line FNN model for estimation and classification flank and crater wear. In order to improve the accuracy of tool wear prediction, they employed AErms, skew, forces, and kurtosis of force bands as network inputs. The results showed that the proposed method of estimating the tool wear achieved high accuracy. Li et al. [19] presented the FNN which is developed and designed to predict tool life in dry milling operation. The proposed FNN integrated a fuzzy logic inference into a NN structure which is basically a multi-layered fuzzy-rule-based neural network. The fuzzy rules improve the accuracy in prediction and assist network to speed up the learning process. Comparing prediction performances with Backpropagation Neural Networks (BPNN), Radial Basis Function Networks (RBFN) and Multi-Regression Models (MRM), the FNN is superior to those methods in prediction accuracy. The uncertainties caused by cutting fluid, environmental conditions and material properties affecting the reliability of the tool wear prediction. Zhang et al. [20] designed a type-2 fuzzy basis function network (FBFN) for tool wear monitoring. The type-2 FBFN is capable of estimating the uncertainty bounds associated with tool wear measurement. The results show that the proposed tool wear model increases accuracy and improves robustness.

The above-mentioned methods used backpropagation (BP) algorithm which employs the gradient descent technique to minimize the error function to adjust network parameters. The BP algorithm has fast convergence ability, but it is liable to trap into the locally optimal solution. To improve the shortcomings of BP, much attention has been paid to adopting evolutionary algorithms to solve the global optimal solution and parameter optimization problems, for instance, genetic algorithm (GA) [21], ant colony optimization (ACO) [22], differential evolution (DE) [23], whale optimization algorithm (WOA) [24], artificial bee colony algorithm (ABC) [25], and particle swarm optimization (PSO) [26-28]. Among them, PSO has been widely applied in various fields as a simple structure, few parameters settings, and superior solving ability. Nevertheless, the conventional PSO still has the disadvantages of unstable convergence and easy to fall into the local optimal solution. In order to address these shortcomings, this paper utilizes a new evolutionary concept to effectively improve the performance of PSO.

The objective of this study is to propose an evolutionary fuzzy neural network (EFNN) for tool wear prediction. The contributions include (1) providing the chip chromaticity coordinate values as one of the feature vectors to predict the tool wear value; (2) proposing an EFNN to establish the tool wear prediction model; (3) designing a dynamic group cooperative particle swarm optimization (DGCPSO) which combines the concepts of dynamic group and cooperative to optimize network parameters. This paper is organized as follows: Section 2 and 3 introduce the experimental equipment and materials as well as the proposed method. Section 4 discusses the experimental results. The last section presents the conclusion and future works.

II. Machining Principle

A. Tool wear theory

During the cutting process, the cutting tool will rub against the workpiece and generate excessive heat. As the cutting continues, the dent will appear on the blade, which is called mechanical wear [29-30]. When the blade of the tool deforms, the cutting resistance increases and temperature increases. It leads to the tool to wear rapidly, which in turn causes the tool to lose the cutting ability [31-32]. Since the degree of tool deterioration determines the end of useful tool life. The International Standards Organization (ISO) standard for tool life evaluation (ISO-8688-1 1994) is adopted to estimate the tool life in this paper. The ISO standard recommends that if the uniform wear of the flank surface reaches 0.3 mm or the uneven wear reaches 0.6 mm, the tool needs to be changed. In the method of formulating tool life, Taylor's tool life equation is often used to represent the relationship between the tool life and the cutting velocity [33-34]. The equation can be expressed as follows:

$$VT^n = C$$

where V presents the cutting velocity (m/min); T denotes the tool life (min); n is the constant depended on the tool material; C is the constant. During the machining process, the machining parameters are considered in the tool life formula. The detail tool life formula with machining parameters (feed per tooth and depth of cut) can be obtained as follows:

$$VT^n f^\alpha d^\beta = C$$

where f presents the feed per tooth (mm/tooth); d is the depth of cut (mm); α and β are the exponential constants.

B. Machining chip colors

The high-speed rotating tool will rub against the material and generate a lot of heat, during the cutting process. The high-temperature chips which cut from the material will rapidly be cooled in the air, and cause the chip to produce an oxide film of different colors on the surface [35-37]. For different chip colors, the cutting temperature is different. The chip color during the cutting process changes in the following order: yellow → brown → purple → blue → blue green.

III. Experimental Equipment and Materials

This section describes the preliminaries including machine tool specification, cutting material,

cutting tool, and industrial camera.

A. Machine tool specification

This paper used the EXTRON SU-85 CNC five-axis processing machine of Yih Chuan machinery industry firm to collect the experimental data. The specifications of the machine are introduced in Figure 1 and Table 1.

Figure 1. Five-axis machine tool (EXTRON SU-85)

Table 1. Specification of machine tool (EXTRON SU-85)

X/Y/Z axes travel [mm]	860 /540 /630
X/Y/Z rapid feed rate [m/min]	30 /30 /240
Spindle speed [rpm]	15,000
Table size [m]	930 x 500
Table load capacity [kg]	400
Machine weight [kg]	6400

B. Cutting material

The 2316MOD stainless steel with a size of 136.5 × 73 mm^2 is used in this study. This cutting material belongs to martensitic crystal structure and it is widely applied in plastic injection molding, extrusion molding or forging process molding. The 2316MOD stainless steel material and mechanical properties are shown in Figure 2 and Table 2.

Figure 2. The workpiece of 2316MOD stainless steel material

Table 2. 2316MOD stainless steel mechanical properties

Coefficient of thermal expansion (10-6 / K)	Thermal Conductivity (W/mK)	Young' s Modulus (kN/mm^2)	Tensile Strength (N/mm^2)	Hardness Brinell (HB)
10	23	215	1350	265~310

C. Cutting tool

The R217.69-3232.0-18-3AN tool holder and XOMX180631TR-ME13 F40M disposable blades are provided by SECO tool manufacturers. The specifications are shown in Tables 3 and 4.

Table 3. SECO tool holder specification

	Specification name	R217.69-3232.0-18-3AN
a_p	Maximum cut depth (mm)	17
D_c	Maximum tool outer diameter (mm)	32
dm_m	Tool holder dianeter (mm)	32
l_p	Tool holder length (mm)	170
l_2	Tool holder total length (mm)	210
RPMX	Maximum RPM (rpm)	11100

Table 4. SECO disposable tool holder bits specification

	Specification name	XOMX180631TR-ME13 F40M
	Materials and coatings	Carbide PVD
EA	Blade clearance angle (°)	15
RA	Blade bevel (°)	30
l	Blade length (mm)	16.5
d	Blade width (mm)	11.2
s	Blade thickness (mm)	6.35

D. Industrial camera

The images are captured by FULL HD 1080p industrial camera of Wenham company. The industrial camera adopts WH-SDI500 CCD which includes 1x~8x shutter, automatic white balance and 84x~560x magnification. The acquired material chip images and measured tool wear values are calculated by the camera software under ML-66 LED light source. Figure 3 presents the industrial camera equipment. As shown in Figure 3 the cutting chip is placed into the center of the platform and then adjust the appropriate magnification to obtain the chip image.

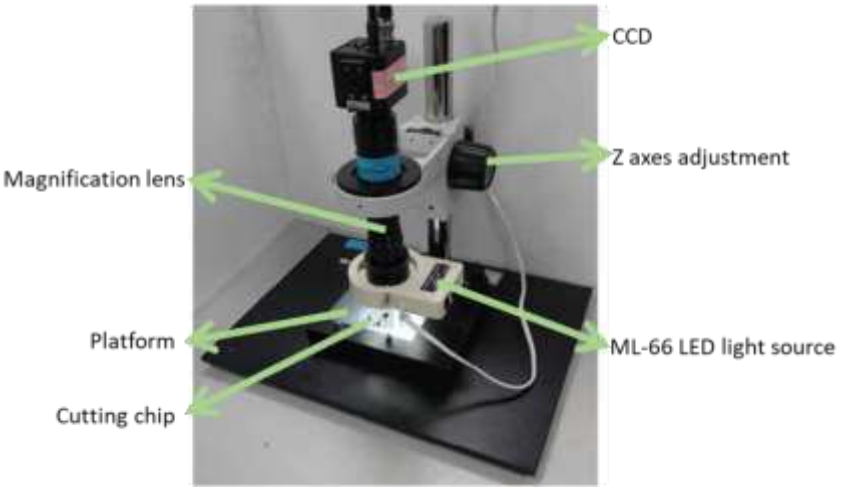

Figure 3. Wenham industrial camera equipment

IV. The framework of EFNN based tool wear prediction method

Tool wear prediction is one of the important applications in the machinery industry. When tool wear occurs, the quality of the product will decline and result in an increase in production cost. The goal of this paper is to develop a prediction framework to provide a more effective and accurate approach for tool wear prediction. The prediction framework consists of three- phase: data collection, chip feature extraction, and EFNN model establishment. Figure 4 shows the corresponding flow chart of the proposed tool wear prediction framework. In the first phase, we chose CNC machining parameters for the cutting experiment and collected experimental data. Next phase, material chip images collected by industrial cameras were calibrated using a color calibration model to obtain more accurate chip images. Subsequently, the calibrated chip image was converted into the CIE *xy* chromaticity values to extract the chip feature. Finally, data-driven and EFNN approaches are applied to establish the tool wear prediction model. The training scheme of EFNN employs the proposed DGCPSO which improves the shortcoming of conventional PSO to increase prediction accuracy. The details about each of the phases are presented as follows.

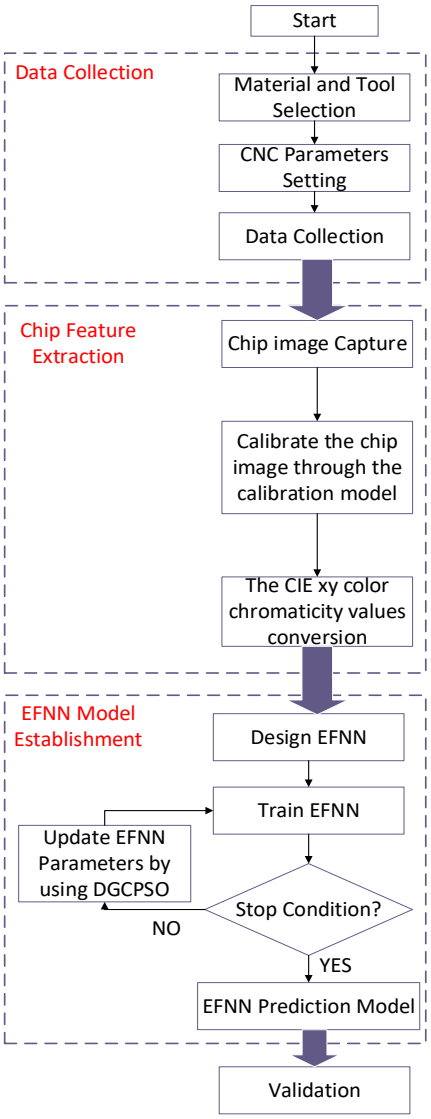

Figure 4. Flow chart of the proposed tool wear prediction framework

A. *Data Collection*

The cutting experiment using the Extron SU-85 CNC machine was performed by employing the selected three experimental trials. Each experimental trial executes seven times cutting process, then ten material chip images with a tool wear value are collected in one cutting process. Thus, a total of 210 training data were collected in ten experimental trials. The testing data selected one experimental trial which consists of a total of 70 testing data. The CNC machining parameters of the cutting experiment were chosen in Table 5.

Table 5. CNC machining parameters in cutting experiment

Parameters	Value
Cutting speed [m/min]	500
Feed per tooth [mm/tooth]	0.1
Depth of cut [mm]	20
Width of cut [mm]	1
Cutting direction	Down milling

B. Material Chip Feature Extraction

After cutting experiment, the chip images were obtained by an industrial camera. The full image (1920×1080) of the chip contains the chip edge, which is unnecessary information. To obtain the chip feature image, a range of 300 × 300 pixels in the center of the image is chosen as the chip feature. The chip feature image is shown in Figure 5.

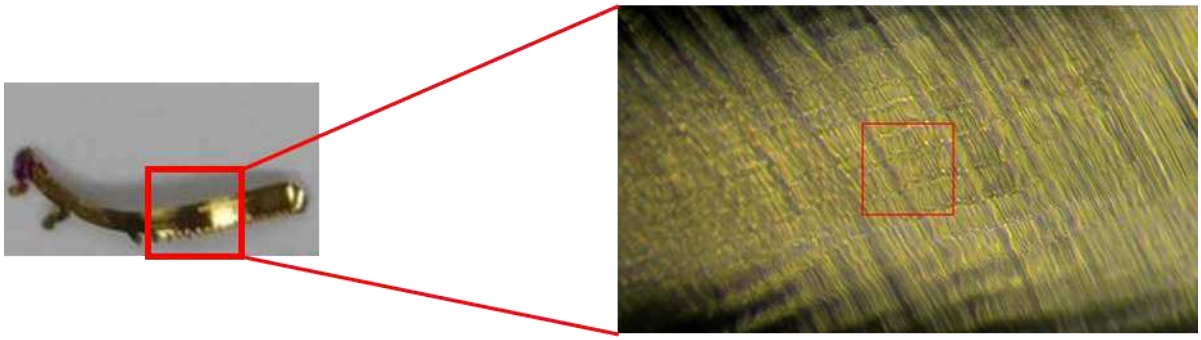

Figure 5. The chip feature image

In the real environment, the brightness, light sources, and color temperature will affect the quality of chip images, causing the color difference. In previous studies [38]-[40], some scholars used regression algorithms to build a color calibration model and adopted color difference to evaluate its performance. Since the color temperature cannot be calculated in the RGB color space, the regression model that converts RGB to the CIELAB color space plays the role of color space conversion. This paper refers to the above method and uses the regression algorithm to establish a color calibration model. The color calibration model which is evaluated by the NBS color difference unit (from the National Bureau of Standards U.S.) is proposed to calibrate the chip feature image [41]. The NBS unit can be divided into six levels as shown in Table 6. In case of the NBS unit of the color calibration model is less than 1.5, it demonstrates that the calibrated color is accurate enough and the color calibration model has been established. Otherwise, the color calibration model should be re-established. The flow chart of establishing color calibration model is shown in Figure 6.

Table 6. National Bureau of Standards (NBS) ratings

NBS unit	Critical remarks of color differences	
0.0 – 0.5	Trace	Extremely slight change
0.5 – 1.5	Slight	Slight change
1.5 – 3.0	Noticeable	Perceivable
3.0 – 6.0	Appreciable	Marked change
6.0 – 12.0	Much	Extremely marked
12.0 or more	Very much	Change to other colour

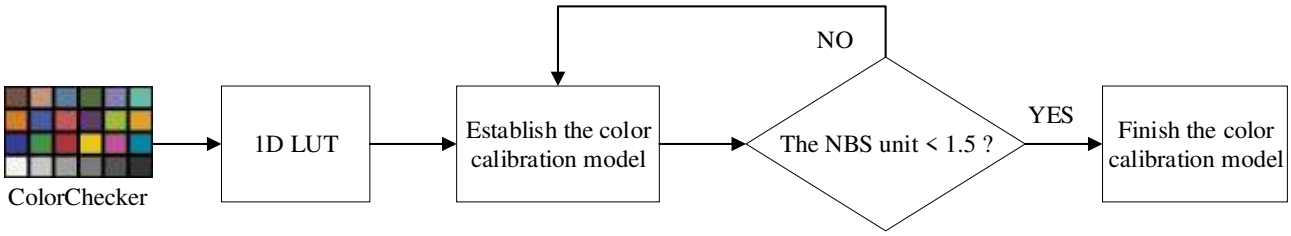

Figure 6. The flow chart of establishing color calibration model

The 1D look-up table (LUT) is used to obtain the adjusted RGB color value (R', G' and B') of the ColorChecker image taken by an industrial camera. Each value of ColorChecker can be found in [42]. The proposed color calibration model was established by adopting the CIELAB color space and regression algorithm. To calculate the color difference, the RGB color space must be converted to CIELAB color space. The regression equation of CIELAB color space transformation is defined as follows.

$$\begin{bmatrix} L_1^* & a_1^* & b_1^* \\ L_2^* & a_2^* & b_2^* \\ \vdots & \vdots & \vdots \\ L_{24}^* & a_{24}^* & b_{24}^* \end{bmatrix} = \begin{bmatrix} 1 & R_1' & G_1' & B_1' & R_1'G_1' & R_1'B_1' & G_1'B_1' & R_1'^2 & G_1'^2 & B_{20}'^2 & R_1'G_1'B_1' & R_1'^3 & G_1'^3 & B_1'^3 \\ 1 & R_2' & G_2' & B_2' & R_2'G_2' & R_2'B_2' & G_2'B_2' & R_2'^2 & G_2'^2 & B_{20}'^2 & R_2'G_2'B_2' & R_2'^3 & G_2'^3 & B_2'^3 \\ \vdots & \vdots & \vdots & \vdots & \vdots & \vdots & \vdots & \vdots & \vdots & \vdots & \vdots & \vdots & \vdots & \vdots \\ 1 & R_{24}' & G_{24}' & B_{24}' & R_{24}'G_{24}' & R_{24}'B_{24}' & G_{24}'B_{24}' & R_{24}'^2 & G_{24}'^2 & B_{24}'^2 & R_{24}'G_{24}'B_{24}' & R_{24}'^3 & G_{24}'^3 & B_{24}'^3 \end{bmatrix} \times \begin{bmatrix} a_0 & b_0 & c_0 \\ a_1 & b_2 & c_1 \\ \vdots & \vdots & \vdots \\ a_{13} & b_{13} & c_{13} \end{bmatrix} \quad (1)$$

where $L^*a^*b^*$ is the standard CIELAB color value in ColorChecker; $R'G'B'$ is the RGB color value adjusted by 1D LUT; a, b, and c are the color calibration parameter. The color difference is calculated by the following equation after the model established.

$$\Delta E_{ab}^* = \sqrt{(L_2^* - L_1^*)^2 + (a_2^* - a_1^*)^2 + (b_2^* - b_1^*)^2} \quad (2)$$

where the ΔE_{ab}^* represents color difference; $L_1^*a_1^*b_1^*$ denotes the standard CIELAB color value in ColorChecker; $L_2^*a_2^*b_2^*$ is the CIELAB color value calibrated by the color calibration model. The ΔE_{ab}^* is then converted to NBS unit to evaluate whether the color calibration model is accurate enough.

$$\text{NBS unit} = \Delta E_{ab}^* * 0.92 \quad (3)$$

In this paper, the CIE *xy* chromaticity coordinate is used as a feature vector of the chip image. The advantage of the CIE *xy* chromaticity coordinate is that it specifies a magnitude-independent hue and purity of a color. A color can be specified uniquely by its *xy* chromaticity coordinate value. Through the color calibration model, the output of chip image is CIELAB color space. Nevertheless, the correlated color temperature of CIELAB is 5000K(D50), which is different from most commonly

artificial daylight 6500K (D65). It is necessary to change the color temperature before convert into the CIE *xy* color space. The color conversion process is shown in Figure 7.

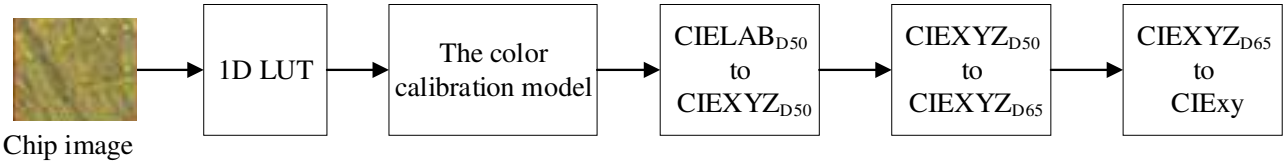

Figure 7. The flow chart of color conversion process

The calibrated chip image is converted to CIEXYZ$_{D50}$ (Tristimulus values) by following equations.

If $L^* > 7.9996$

$$X_{D50} = 96.42 \times (\frac{a^*}{500} + \frac{L^*+16}{116})^3 \quad Y_{D50} = 100 \times (\frac{L^*+16}{116})^3 \quad Z_{D50} = 82.49 \times (\frac{L^*+16}{116} - \frac{b^*}{200})^3 \tag{4}$$

else

$$X_{D50} = \frac{96.42}{7.787} \times (\frac{a^*}{500} + \frac{L^*}{116}) \quad Y_{D50} = \frac{a^*}{903.292} \quad Z_{D50} = \frac{82.49}{7.787} \times (\frac{L^*}{116} - \frac{b^*}{200}) \tag{5}$$

where $L^*a^*b^*$ is the CIELAB color value; XYZ_{D50} is the CIEXYZ color value of color temperature 5000K. Then, the color temperature D50 is converted to D65 by the following equation.

$$[X_{D65} \quad Y_{D65} \quad Z_{D65}] = [X_{D50} \quad Y_{D50} \quad Z_{D50}] \begin{bmatrix} 0.9556 & -0.0284 & 0.0124 \\ -0.0232 & 1.0101 & -0.0206 \\ 0.0633 & 0.0211 & 1.3306 \end{bmatrix} \tag{6}$$

The calibrated image of the chip is obtained by converting CIEXYZD65 into CIExy color space. The equation is defined as follows.

$$CIEx = \frac{X_{D65}}{X_{D65}+Y_{D65}+Z_{D65}} \quad CIEy = \frac{Y_{D65}}{X_{D65}+Y_{D65}+Z_{D65}} \tag{7}$$

Finally, each pixel of the image is added and averaged to acquire the chromaticity feature.

$$x = \frac{\sum_1^n CIEx_i}{n} \quad y = \frac{\sum_1^n CIEy_i}{n} \tag{8}$$

where n is the total number of image pixel.

C. EFNN prediction model

This subsection introduces the proposed EFNN model for tool wear prediction. Compared to conventional NN, the proposed EFNN has the following advantages: (1). The EFNN combines the fuzzy logic (FL) and functional link neural network (FLNN) to avoid overfitting problems. (2). The EFNN can reasonably remove noises from the internal rules by proper fuzzy treatment. (3). The ability to approximate the nonlinear function. The proposed EFNN model is divided into two parts: (1) EFNN architecture; (2) DGCPOS learning algorithm. Figure 8. shows the block diagram of the tool wear prediction model. Through feature extraction, the chip CIE *xy* chromaticity value is obtained, and then the CIE *xy* chromaticity value and cutting time are input into EFNN to acquire the tool wear

value.

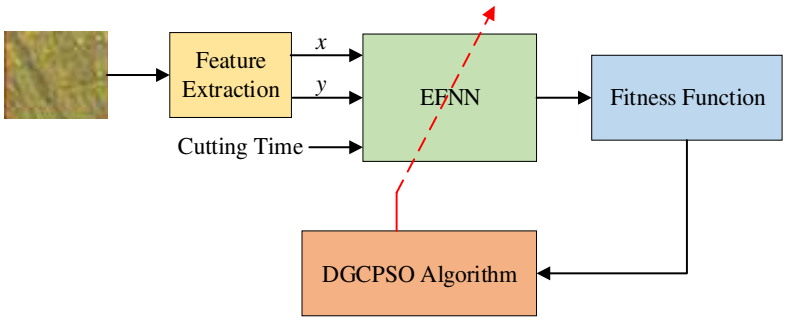

Figure 8. Tool wear prediction model architecture diagram

1. Evolutionary fuzzy neural network

Figure 9 presents the architecture of an EFNN which consists of an input layer, a membership function layer, a firing layer, a consequent layer, and an output layer. The IF-THEN rule can be expressed as follows.

$$\text{Rule}_j : \text{IF } x_1 \text{ is } A_{1j} \text{ and } x_2 \text{ is } A_{2j} \ \ldots \text{and } x_i \text{ is } A_{ij}$$

$$\text{THEN } y_j = \sum_{k=1}^{M} \omega_{kj}\varphi_k = \omega_{1j}\varphi_1 + \omega_{2j}\varphi_2 + \cdots + \omega_{Mj}\varphi_M$$

where x_i presents the input; y_j is the output; A_{ij} represents the interval type-2 fuzzy sets; $j = 1, 2, \ldots, R$ represents the rule number; ω_{kj} is the link weight; φ_k represents the basis trigonometric function, and M is the number of basis functions.

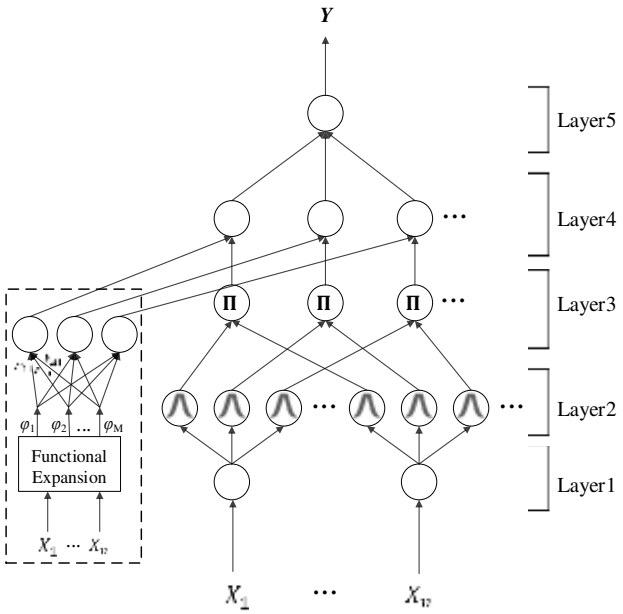

Figure 9. Evolutionary fuzzy neural network architecture

In layer 2, each interval type-2 fuzzy set (A_{ij}) uses the following Gaussian primary membership function which has an uncertainty mean $[m_{ij1}, m_{ij2}]$ and standard deviation σ_{ij}.

$$u_{ij}^{(2)} = exp\left(-\frac{\left[u_i^{(1)} - m_{ij}\right]^2}{\sigma_{ij}^2}\right) \equiv N(m_{ij},\ \sigma_{ij};\ u_i^{(1)}),\ m_{ij} \in \left[m_{ij}^{(1)},\ m_{ij}^{(2)}\right] \tag{9}$$

where m_{ij} and σ_{ij} are the mean and standard deviation. The type 2 Gaussian membership function consists of upper boundary $\overline{u}_{ij}^{(2)}$ and the lower boundary $\underline{u}_{ij}^{(2)}$, as shown in the following equation.

$$\overline{u}_{ij}^{(2)} = \begin{cases} N\left(m_{ij}^{(1)}, \sigma_{ij};\ u_i^{(1)}\right), & if \quad u_i^{(1)} < m_{ij}^{(1)} \\ 1\ , & if \quad m_{ij}^{(1)} \le u_i^{(1)} \le m_{ij}^{(2)} \\ N\left(m_{ij}^{(2)}, \sigma_{ij};\ u_i^{(1)}\right), & if \quad u_i^{(1)} > m_{ij}^{(2)} \end{cases}$$

$$\underline{u}_{ij}^{(2)} = \begin{cases} N\left(m_{ij}^{(2)}, \sigma_{ij};\ u_i^{(1)}\right), if & u_i^{(1)} \le \frac{m_{ij}^{(1)} + m_{ij}^{(2)}}{2} \\ N\left(m_{ij}^{(1)}, \sigma_{ij};\ u_i^{(1)}\right), if & u_i^{(1)} > \frac{m_{ij}^{(1)} + m_{ij}^{(2)}}{2} \end{cases} \tag{10}$$

The firing strengths $\overline{u}_j^{(3)}$ and $\underline{u}_j^{(3)}$ of each rule node in layer 3 are computed by algebraic product operation.

$$\overline{u}_j^{(3)} = \prod_i \overline{u}_{ij}^{(2)} \text{ and } \quad \underline{u}_j^{(3)} = \prod_i \underline{u}_{ij}^{(2)} \tag{11}$$

where $\prod_i \overline{u}_{ij}^{(2)}$ and $\prod_i \underline{u}_{ij}^{(2)}$ represent the firing strength of the interval's upper bound and lower bound. Then the type-2 fuzzy set is transformed into type-1 fuzzy set by using the method of reduction of order. The method is described as follows.

$$\overline{u}^{(4)} = \frac{\sum_{j=1}^{R} \overline{u}_j^{(3)} (\sum_{k=1}^{M} \omega_{kj} \varphi_k)}{\sum_{j=1}^{R} \overline{u}_j^{(3)}}, \underline{u}^{(4)} = \frac{\sum_{j=1}^{R} \underline{u}_j^{(3)} (\sum_{k=1}^{M} \omega_{kj} \varphi_k)}{\sum_{j=1}^{R} \underline{u}_j^{(3)}} \tag{12}$$

where $\sum_{k=1}^{M} \omega_{kj} \varphi_k$ is a nonlinear combination of EFNN inputs; the functional expansion is based on basis trigonometric functions and defined as follows.

$$[\varphi_1, \varphi_2, \cdots, \varphi_M] = [x_1, \sin(\pi x_1), \cos(\pi x_1), \cdots, x_n, \sin(\pi x_n), \cos(\pi x_n)] \tag{13}$$

where $\mathrm{M} = 3 \times \mathrm{n}$ is the number of basis functions and n is the number of inputs. After the reduction process, the output is defuzzified by computing the average of $\overline{u}^{(4)}$ and $\underline{u}^{(4)}$. The crisp value y is obtained as follows.

$$y = \frac{\overline{u}^{(4)} + \underline{u}^{(4)}}{2} \tag{14}$$

2. *DGCPOS learning algorithm*

The traditional PSO algorithm has the advantages of fast convergence and simple implementation, but in the complex problems, the precision is not enough and easy trap into a locally optimal solution. A dynamic group cooperative particle swarm optimization is proposed to boost the learning efficiency of EFNN. Different from the traditional evolution method, the cooperative method split P particles into N sub-vectors for evolution, which solve a one-dimension optimization problem. Figure 10-11 shows the differences between traditional and cooperative evolution methods. The cooperative method can effectively improve the convergence speed, but it takes more computing time and is easily fall into a suboptimal solution. To overcome that shortcoming, the dynamic group strategy is also introduced to enhance the searching ability of the global optimal solution. In the DGPSO algorithm, each particle will be grouped through a dynamic group strategy and selected the best fitness particle as the leader. Only leader particles of each group are evolved by using the cooperative method, which can reduce the computational complexity and avoid falling into a suboptimal solution. The flowchart of the proposed DGCPSO algorithm is shown in Figure 12.

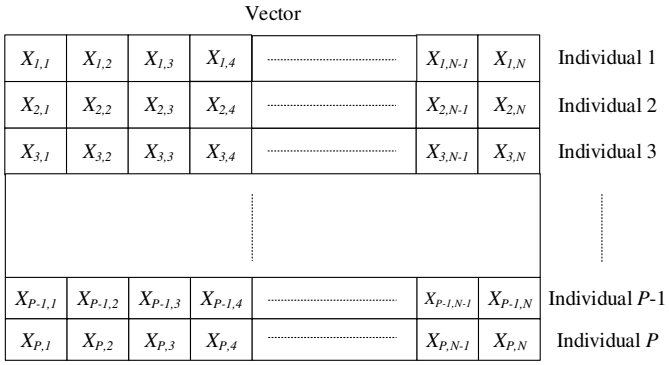

Figure 10. Traditional evolution method

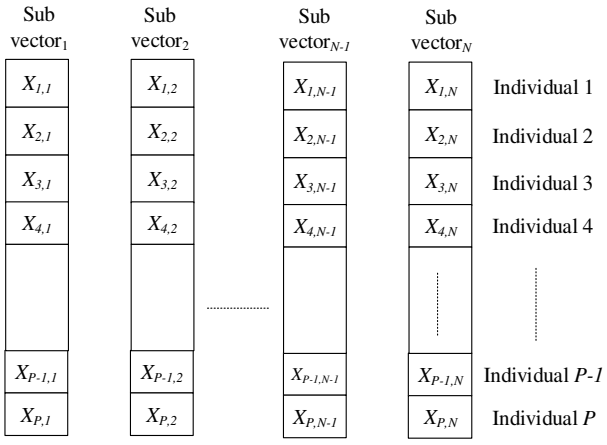

Figure 11. Cooperative evolution method

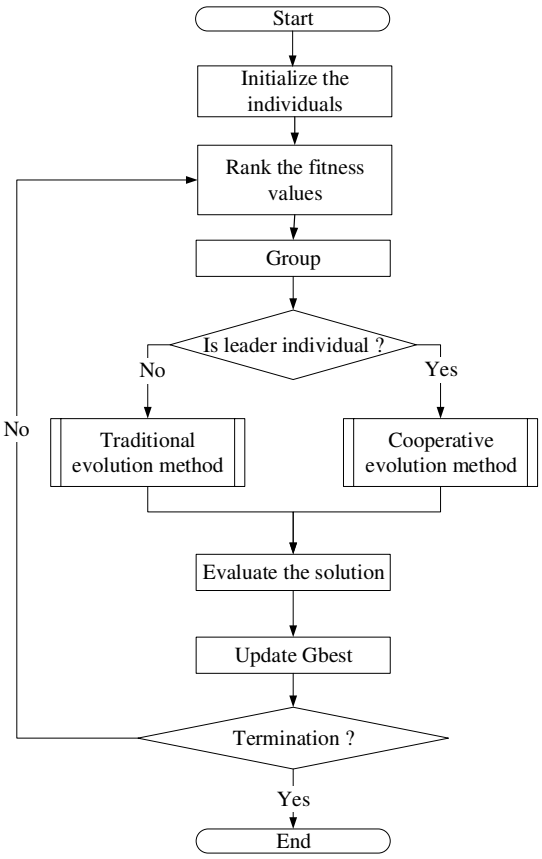

Figure 12. The flowchart of the proposed DGCPSO algorithm

All the EFNN parameters are coded into a particle that contain uncertainty mean m_{ij}, standard deviation σ_{ij}, and consequence link weights ω_{kj}. The fitness values of all particles are ranked in descending order and the initial group number is set as 0, as shown in Figure 12.

Group :	0	0	⋯	0	0	⋯	0	0
Individual :	X_1	X_2	⋯	X_i	X_{i+1}	⋯	X_{NP-1}	X_{NP}
Fitness :	Best				→			Worst

Figure 12. Ranking the order of particles

The particle with the highest fitness value will be set as the leader of the new group and the group number is updated from zero to one. Then calculate the distance threshold and fitness threshold the of each particle that is ungrouped by following equations.

$$\delta_k = \frac{\sum_{i=1}^{P}\sum_{j=1}^{D}\sqrt{(L_{kj}-X_{ij})^2}}{NG} \tag{15}$$

$$\psi_k = \frac{\sum_{i=1}^{P}|F(L_k)-F(X_i)|}{NG} \tag{16}$$

where δ_k and ψ_k represent the distance threshold and fitness threshold; *P* and *N* are the encoded dimension and the total number of particle, respectively; $L_{k,j}$ represents the k*th* group leader with the j*th* dimension; $F(\cdot)$ denote the fitness function; *NG* represents the total number of ungrouped particle. The distance values and fitness values between the ungrouped particles and the leader particles are calculated as follows.

$$\mathcal{D}_i = \sum_{j=1}^{D} \sqrt{(L_{kj} - X_{ij})^2} \tag{17}$$

$$\mathcal{F}_i = |Fitness(L_k) - Fitness(X_i)| \tag{18}$$

The particle is similar to the *g*th group leader, if $\mathcal{D}_i$ and $\mathcal{F}_i$ are less then δ_k and ψ_k. The group number of these particles is updated to g. The grouping process is completed until no ungroup particles exist. The evolution process is divided into traditional evolution and cooperative evolution method, respectively. Two evolution methods are introduced in detail as follows.

- Traditional evolution method

To overcome the shortcomings of traditional PSO algorithms, this study proposes a new position update method. The particles no longer refer the personal best position, but instead refer to leader particle L_g in their group. The position update formula is as follows:

$$V_i(n+1) = \omega \times V_i(n) + C_1 \times rand_1 \times \left(L_g - X_i(n)\right) + C_2 \times rand_2 \times \left(P_{Gbest} - X_i(n)\right) \tag{19}$$

$$X_i(n+1) = X_i(n) + V_i(n+1) \tag{20}$$

where $V_i(n)$ represents the particle velocity, $X_i(n)$ is the current position of the particle, P_{Gbest} is the global best value of all particles, ω is the inertia weight, C_1 represents the cognitive parameter, C_2 represents the social parameter, and $rand_1$ and $rand_2$ are random numbers between 0 and 1.

- Cooperative evolution method

The leader particles are split into *N* sub-vectors of one-dimension. Each sub-vector will pick out the best particle of one-dimensional. Until the *N*th element of the P_{Gbest} particle is replaced by each sub-vector of the *P*th particle in turn, the other elements of the P_{Gbest} particle remain constant values. After the above process, the new global best particle L_{best} can be obtained. All the leader particles are updated with reference to L_{best} in the following equation.

$$V_i(n+1) = \omega \times V_i(n) + C_1 \times rand_1 \times \left(P_i - X_i(n)\right) + C_2 \times rand_2 \times \left(L_{best} - X_i(n)\right) \quad (21)$$

$$X_i(n+1) = \ X_i(n) + V_i(n+1) \quad (22)$$

where P_i is the personal best solution of the *i*th leader particle. If the terminal condition is satisfied, end the learning process. Otherwise, continue the learning process.

V. Experimental results

The experimental results are demonstrated in two parts. Firstly, the relationship between chip color and tool wear value through cutting experiments as well as the Pearson's correlation coefficient for verifying the relationship between those two factors are discussed. Secondly, the proposed EFNN is used to predict the tool wear value and the predicted results are compared with different evolutionary algorithms.

A. Material chip data analysis

Four datasets were obtained after the cutting experiments including three training datasets and one testing dataset as shown in Figure 13. Tool wear status can be divided into three stages: initial wear, steady wear and accelerated wear. In the initial wear stage, the chip color presents golden yellow. As the cutting time increases, the tool enters into a steady wear stage which causes the chip color turning into dark yellow. After the fifth cutting process, the tool suffers from accelerated wear and the chip appears burnt yellow. These phenomena indicate that different tool wear values result in different colors of chips. As displayed in Figure 13, the tool wear values of four datasets show a consistent trend in three wear states. Furthermore, when the tool wear value exceeds 0.3 mm, the tool life is end and the tool needs to be changed.

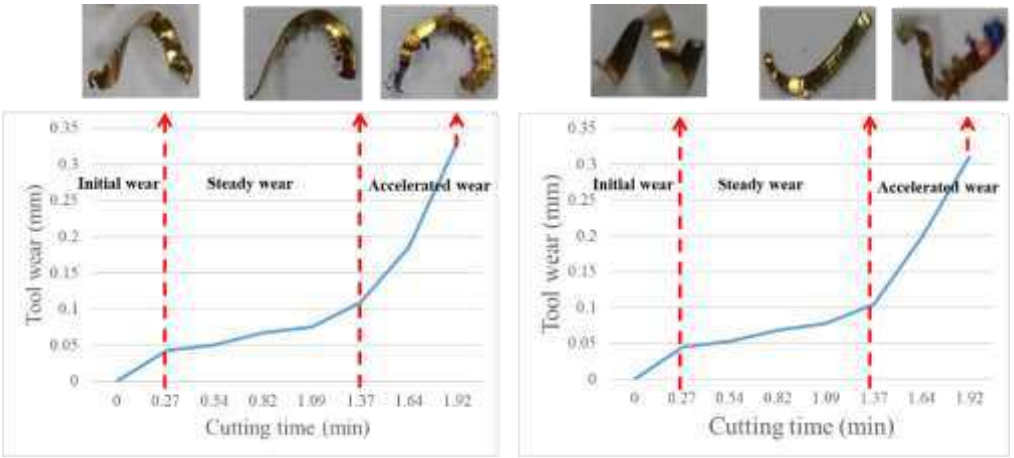

(a) Training dataset 1 (b) Training dataset 2

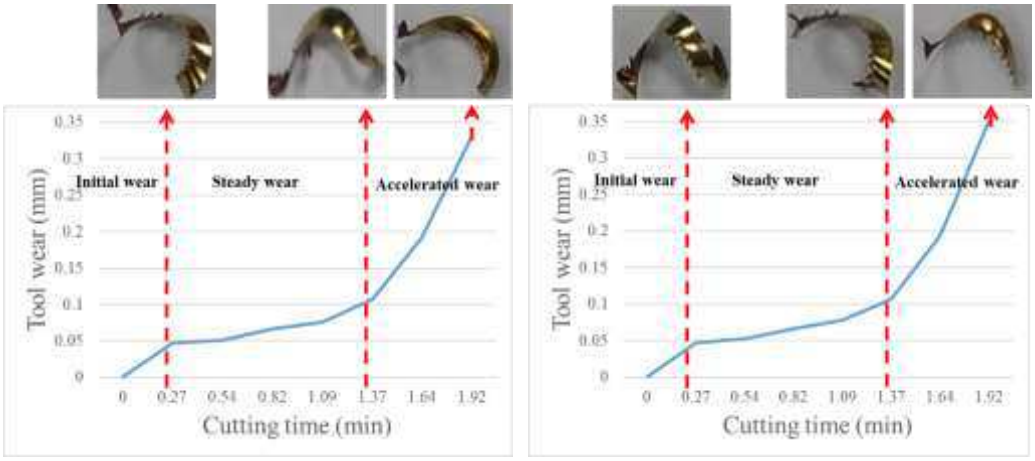

(c) Training dataset 3 (b) Testing dataset

Figure 13. The datasets of cutting experiments

Meanwhile, the Pearson's correlation coefficient is also used to analyze the relationship between the CIE xy chromaticity value and tool wear value in this paper. The definition of Pearson's correlation coefficient is shown as follows.

$$r_{ab} = \frac{\sum_{i=1}^{n}(a_i-\overline{a})(b_i-\overline{b})}{\sqrt{\sum_{i=1}^{n}(a_i-\overline{a})^2}\sqrt{\sum_{i=1}^{n}(b_i-\overline{b})^2}} \tag{23}$$

where n is sample size; a_i and b_i represent the ith individual sample; $\overline{a}$ and $\overline{b}$ donate the sample mean. The higher r value presents the higher positive correlation between the two variables. Table 7 shows the correlation regarding the CIE xy chromaticity value and tool wear value. In Table 7, the r values of the x chromaticity value and y chromaticity value are 0.709 and 0.512, respectively, which indicates that x chromaticity has higher positive correlation to tool wear than y chromaticity. Though y chromaticity value has only a moderately positive correlation to the tool wear value the CIE xy chromaticity value is still related to the tool wear value.

Table 7. Pearson's correlation coefficient table of two variables

Variable a	Variable b	Pearson's r
x chromaticity	tool wear	0.709
y chromaticity	tool wear	0.512

B. Tool wear prediction results

In artificial network training methods, the backpropagation algorithm is the most commonly used algorithm for training the artificial neural network. However, backpropagation has the problem of falling into a local optimal solution. Some scholars use evolutionary algorithms to replace the backpropagation method and compare its effectiveness [43-45]. They indicate that evolutionary algorithms can not only solve the problem of limited optimization effect and local convergence but also improve the accuracy of prediction. To demonstrate the prediction effectiveness of the proposed DGCPSO, the DGCPSO was compared with BPNN [9], PSO [26], QPSO [27] and CPSO [28] in this

experiment. The initial parameters of the proposed DGCPSO including number of particles, inertia weight *w*, acceleration constant C_1 and C_2, generation and number of fuzzy rules are listed in Table 8.

Table 8. Initial parameters of DGCPSO

Parameters	Value
Particle	30
Inertia weight *w*	0.3
C_1	2
C_2	2
Generation	500
Fuzzy rule	4,5,6

The DGCPSO is evaluated 10 times to ensure search stability for the solution. During the training process, the reciprocal root mean square error (RMSE) is used as a fitness function. The high fitness value implies a better solution. The fitness function is defined as follows.

$$\mathrm{F} = \frac{1}{RMSE+1} \tag{24}$$

$$\mathrm{RMSE} = \sqrt{\frac{\sum_{i=1}^{N}(\hat{y}_i - y_i)^2}{N}} \tag{25}$$

In the EFNN, the user needs to set the number of rules. The number of fuzzy rules is difficult to determine depending on different problems. However, different number of rules will result in different prediction accuracy. More fuzzy rules require more memory space and computation time. Conversely, fewer fuzzy rules will lead to unsatisfactory performance. In this experiment, 4, 5, and 6 fuzzy rules were used to evaluate the efficiency of EFNN. In Table 9, the performance of five fuzzy rules is better than that of four and six; thus, five fuzzy rules are selected to establish the tool wear prediction model in this paper.

Table 9. Effectiveness evaluation of different fuzzy rule

Number of rules / Fitness value	4	5	6
Best fitness value	0.988707	0.991587	0.990425
Worst fitness value	0.955493	0.964216	0.954232
Average fitness value	0.978293	0.982429	0.976923
SD	0.010577	0.008454	0.012037

The evaluation results are calculated using the mean absolute percentage error (MAPE). The definition of MAPE is shown in the following equation.

$$\mathrm{MAPE} = \frac{100\%}{n}\sum_{i=1}^{n}\left|\frac{y_i - \hat{y}_i}{y_i}\right| \tag{26}$$

where n is total number of data; y_i represents the actual output; $\hat{y}_i$ is prediction output. Figure 14 illustrates the predicted results implemented by different algorithms. The axis "number of data" represents the number of total testing data. The testing experimental trial executes seven times cutting process, then ten material chip images with a tool wear value are collected in one cutting process. Thus, a total of 70 testing data were obtained. In Figure 14 (a), BPNN has good accuracy in the first 40 ratios, but it performs poorly in the second half. In contrast, PSO performed well accuracy in the last 30 ratios. Figure 14 (c) and (d) show the oscillating prediction results in each step of QPSO and CPSO. The proposed DGCPSO algorithm introduces the dynamic group mechanism that can address the shortcomings of traditional evolutionary algorithms and improve the searching ability of the global optimal solution. Therefore, in Figure 14 (e), the proposed DGCPSO method performs well accuracy results in testing data. The MAPE value of each algorithm is shown in Table 10. Then as well, the proposed method reaches the smallest MAPE. To illustrate the distribution of tool wear prediction results, the boxplot is used as shown in Figure 15. As displayed in Figure 15, the proposed DGCPSO has a lower distribution of responses than other algorithms. It indicates that the proposed method is relatively stable in tool wear prediction and suitable for establishing the prediction model.

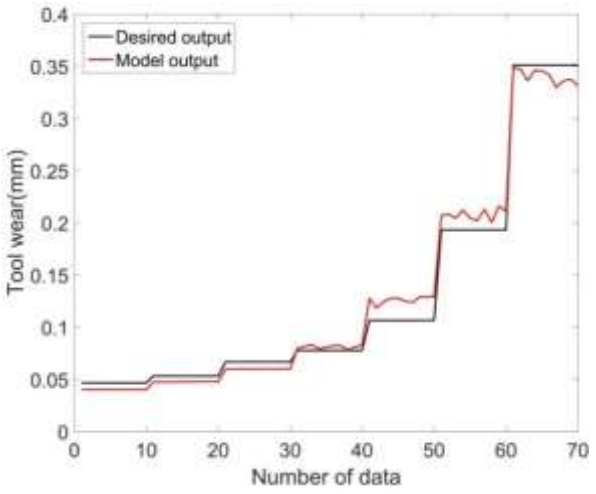

(a) BPNN

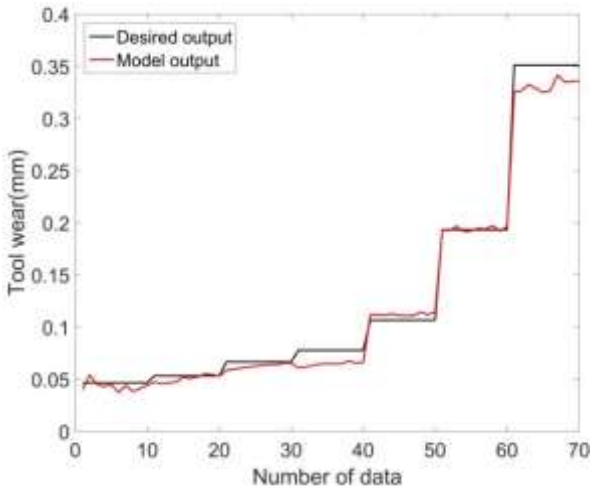

(b) PSO

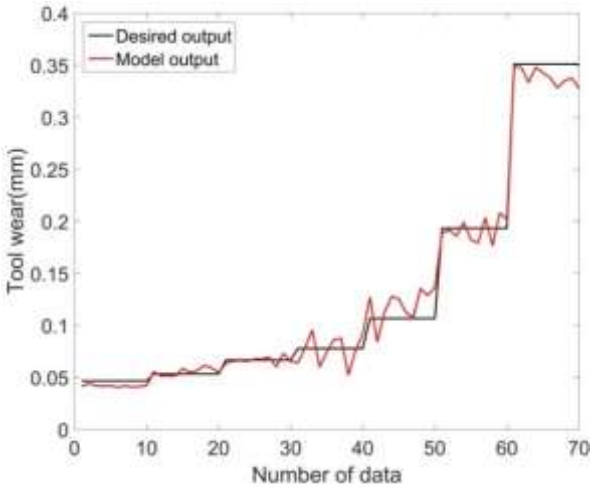

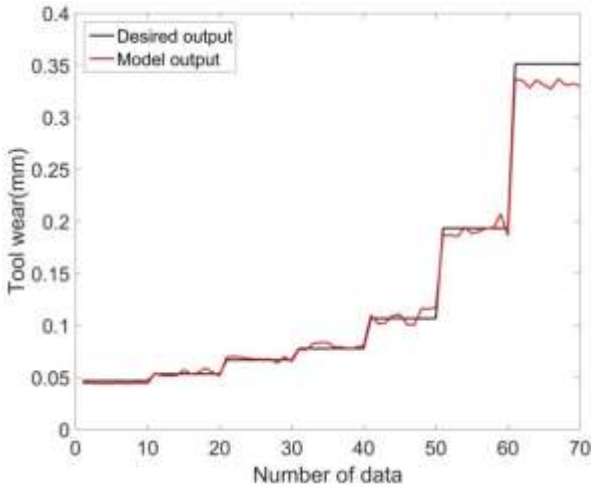

(c) QPSO (d) CPSO

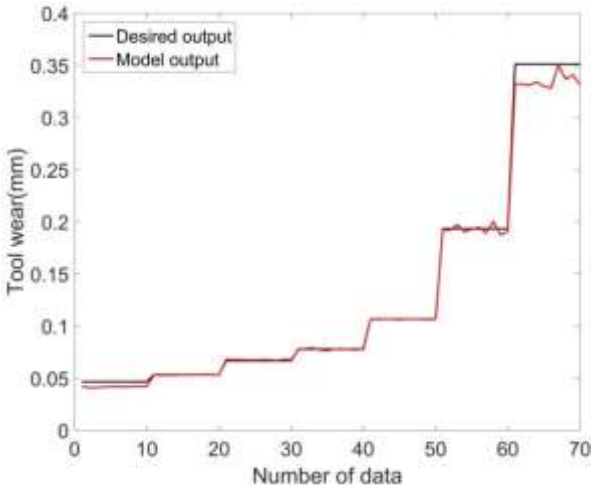

(e) DGCPSO

Figure 14. The prediction results of different algorithms

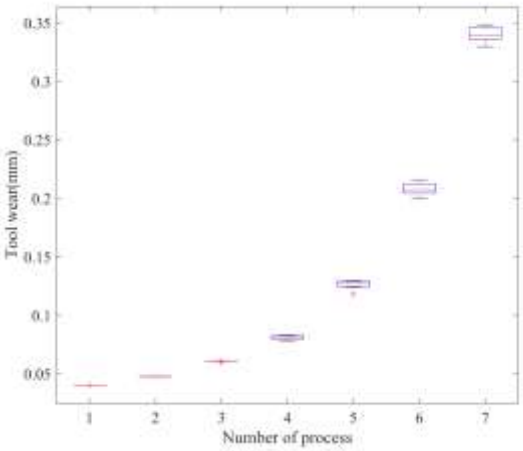

(a) BPNN

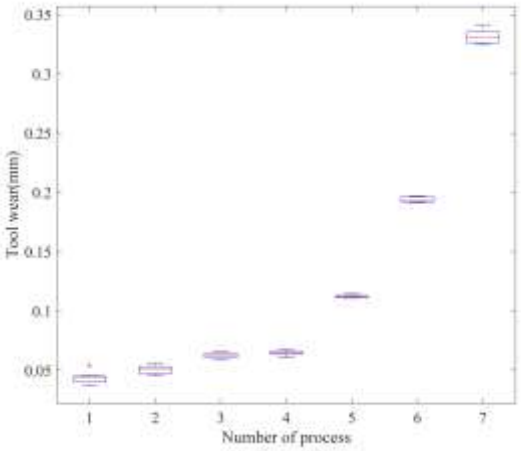

(b) PSO

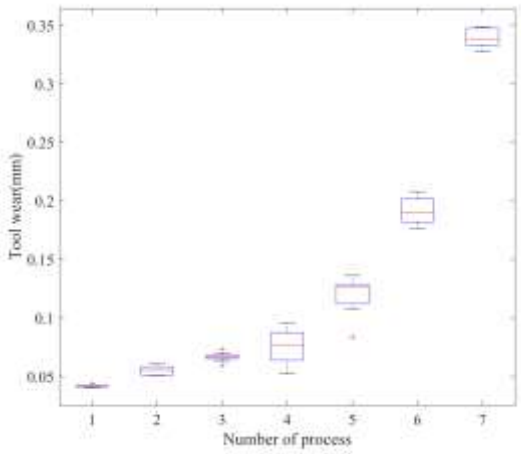

(c) QPSO

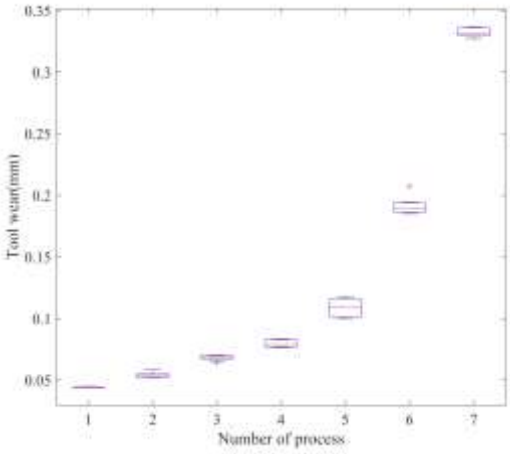

(d) CPSO

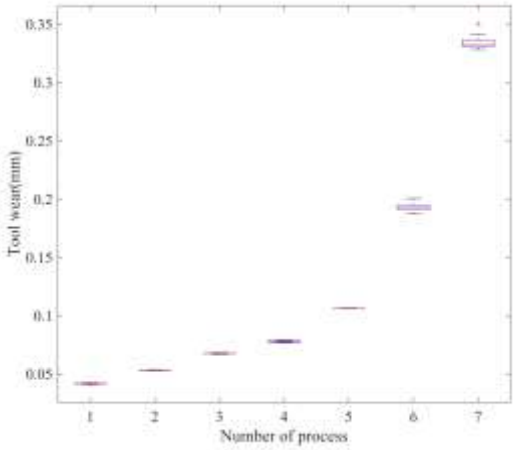

(e) DGCPSO

Figure 15. The boxplot of different algorithms

Table 10. Effectiveness evaluation of different algorithms

Method	MAPE
BPNN	9.72%
PSO	7.42%
QPSO	8.59%
CPSO	4.09%
DGCPSO	2.83%

VI. Conclusion

In the machining process, tool wear directly affects processing quality and cost. It is important

to replace processing tools in time. This paper proposes a tool wear prediction method using material chip chromaticity which replaces the indirect method of using sensors to capture signals. The major contributions of this paper are described as follows:

- Due to color temperature will affect the quality of chip images, causing the color difference. This paper developed the color calibration model by using the regression algorithm to reduce the color difference. The calibrated color difference ΔE_{ab}^{*} is less than 1.5.
- A new EFNN which combines fuzzy logic (FL) and functional link neural network (FLNN) is proposed to establish the tool wear prediction model.
- The proposed DGCPSO used a hybrid method that involves a dynamic group strategy and cooperative concept to overcome the drawbacks of easily trapped into local optimal in the traditional PSO algorithm.
- In the prediction experiment, the proposed EFNN with DGCPSO algorithm performs the smallest MAPE result 2.83% then BPNN 9.72%, PSO 7.42%, QPSO 8.59%, and CPSO 4.09%. It means that the proposed EFNN has a high prediction accuracy and is usable in tool wear prediction.

Authors' contributions

Conceptualization, C.-J.L.; methodology, C.-J.L. and J.-Y.J.; software, C.-J.L., J.-Y.J., and S.-H.C.; data curation, J.-Y.J., and S.-H.C.; writing-original draft preparation, C.-J.L. and J.-Y.J.; funding acquisition, C.-J.L. All authors have read and agreed to the published version of the manuscript.

Funding

This research was funded by the Ministry of Science and Technology of the Republic of China, grant number MOST 109-2218-E-005-002.

Data availability The author confirms that the data supporting the findings of this study are available within the paper.

Compliance with ethical standards

Conflict of interest The authors declare that they have no conflict of interest.

Code availability Not applicable

References

[1] Debnath S., Reddy M.M., Yi Q.S., 2016, Influence of cutting fluid conditions and cutting

parameters on surface roughness and tool wear in turning process using Taguchi method. Measurement, 78:111-9. https://doi.org/10.1016/j.measurement.2015.09.011.

[2] Bar-Hen M., Etsion I., 2017, Experimental study of the effect of coating thickness and substrate roughness on tool wear during turning. Tribology International,110:341-7. https://doi.org/10.1016/j.triboint.2016.11.011.

[3] Zhu K, Zhang Y., 2019, A generic tool wear model and its application to force modeling and wear monitoring in high speed milling. Mechanical Systems and Signal Processing,115:147-61. https://doi.org/10.1016/j.ymssp.2018.05.045.

[4] Kong D., Chen Y., Li N., 2017, Force-based tool wear estimation for milling process using Gaussian mixture hidden Markov models. The International Journal of Advanced Manufacturing Technology, 92:2853-65. https://doi.org/10.1007/s00170-017-0367-1.

[5] Stavropoulos P., Papacharalampopoulos A., Vasiliadis E., Chryssolouris G., 2016, Tool wear predictability estimation in milling based on multi-sensorial data. The International Journal of Advanced Manufacturing Technology, 82:509-21. https://doi.org/10.1007/s00170-015-7317-6.

[6] Madhusudana C.K., Kumar H., Narendranath S., 2016, Condition monitoring of face milling tool using K-star algorithm and histogram features of vibration signal. Engineering Science and Technology, an International Journal,19:1543-51. https://doi.org/10.1016/j.jestch.2016.05.009.

[7] Zhu Z., Sun J., Li J., Huang P., 2016, Investigation on the influence of tool wear upon chip morphology in end milling titanium alloy Ti6Al4V. The International Journal of Advanced Manufacturing Technology, 83:1477-85. https://doi.org/10.1007/s00170-015-7690-1.

[8] Prakash M., Kanthababu M., Rajurkar K.P., 2015, Investigations on the effects of tool wear on chip formation mechanism and chip morphology using acoustic emission signal in the microendmilling of aluminum alloy. The International Journal of Advanced Manufacturing Technology, 77:1499-511. https://doi.org/10.1007/s00170-014-6562-4.

[9] Corne R., Nath C., El Mansori M., Kurfess T., 2017, Study of spindle power data with neural network for predicting real-time tool wear/breakage during inconel drilling. Journal of Manufacturing Systems, 43:287-95. https://doi.org/10.1016/j.jmsy.2017.01.004.

[10] Yao Y., Li X., Yuan Z., 1999, Tool wear detection with fuzzy classification and wavelet fuzzy neural network. International Journal of Machine Tools and Manufacture, 39:1525-38. https://doi.org/10.1016/S0890-6955(99)00018-8.

[11] Zadeh LA., 1997, Toward a theory of fuzzy information granulation and its centrality in human reasoning and fuzzy logic. Fuzzy Sets and Systems, 90:111-27.

[12] Zadeh LA., 2002, Toward a perception-based theory of probabilistic reasoning with imprecise probabilities. Journal of Statistical Planning and Inference, 105:233-64.

[13] Thiele H., 2002, On Algebraic Foundations of Information Granulation. In: Bouchon-Meunier B, Gutiérrez-Ríos J, Magdalena L, Yager RR, editors. Technologies for Constructing Intelligent Systems 1: Tasks. Heidelberg: Physica-Verlag HD., p. 113-26.

[14] Tanaka K, Wang O., 2002, Fuzzy Control Systems Design and Analysis: A Linear Matrix Inequality Approach., p. 5-48.

[15] Chin-Teng L, Chang-Mao Y, Sheng-Fu L, Jen-Feng C, Kumar N., 2006, Support-vector-based fuzzy neural network for pattern classification. IEEE Transactions on Fuzzy Systems., 14:31-41.

[16] Al-Mahasneh M, Aljarrah M, Rababah T, Alu'datt M., 2016, Application of Hybrid Neural Fuzzy System (ANFIS) in Food Processing and Technology. Food Engineering Reviews., 8:351-66.

[17] Zhang L, Yang G-H., 2020, Adaptive fuzzy fault compensation tracking control for uncertain nonlinear systems with multiple sensor faults. Fuzzy Sets and Systems., 392:46-59.

[18] Chungchoo C., Saini D., 2002, On-line tool wear estimation in CNC turning operations using fuzzy neural network model. International Journal of Machine Tools and Manufacture, 42:29-40. https://doi.org/10.1016/S0890-6955(01)00096-7.

[19] Li X., Lim B., Zhou J.H., Huang S., Phua S.J., Shaw K.C., 2009, Fuzzy neural network modelling for tool wear estimation in dry milling operation. Annual Conference of the Prognostics and Health Management Society, PHM 2009.

[20] Zhang B., Katinas C., Shin Y.C., 2018, Robust Tool Wear Monitoring Using Systematic Feature Selection in Turning Processes With Consideration of Uncertainties. Journal of Manufacturing Science and Engineering,140. https://doi.org/10.1115/1.4040267.

[21] Pratama M., Er M.J., Li X., Gan O.P., Oentaryo R.J., Linn S., 2011, Tool wear prediction using evolutionary Dynamic Fuzzy Neural (EDFNN) Network. IECON 2011 - 37th Annual Conference of the IEEE Industrial Electronics Society, 4739-44. https://doi.org/10.1109/IECON.2011.6119997.

[22] Ping G., Chunbo X., Yi C., Jing L., Yanqing L., 2014, Adaptive ant colony optimization algorithm. 2014 International Conference on Mechatronics and Control (ICMC), 95-8. https://doi.org/10.1109/ICMC.2014.7231524.

[23] Gong W., Cai Z., 2013, Differential Evolution With Ranking-Based Mutation Operators. IEEE Transactions on Cybernetics, 43:2066-81. https://doi.org/10.1109/TCYB.2013.2239988

[24] Mirjalili S., Lewis A., 2016, The Whale Optimization Algorithm. Advances in Engineering Software, 95:51-67. https://doi.org/10.1016/j.advengsoft.2016.01.008.

[25] Chen X., Wei X., Yang G., Du W., 2020, Fireworks explosion based artificial bee colony for numerical optimization. Knowledge-Based Systems, 188:105002. https://doi.org/10.1016/j.knosys.2019.105002.

[26] Wang D., Tan D., Liu L., 2018, Particle swarm optimization algorithm: an overview. Soft Computing, 22:387-408. https://doi.org/10.1007/s00500-016-2474-6.

[27] Ho S.L., Yang S., Ni G., Huang J., 2013, A Quantum-Based Particle Swarm Optimization Algorithm Applied to Inverse Problems. IEEE Transactions on Magnetics, 49:2069-72. https://doi.org/10.1109/TMAG.2013.2237760.

[28] Bergh Fvd, Engelbrecht A.P., 2004, A Cooperative approach to particle swarm optimization. IEEE Transactions on Evolutionary Computation, 8:225-39. https://doi.org/10.1109/TEVC.2004.826069.

[29] Leone C, D'Addona D, Teti R., 2011, Tool wear modelling through regression analysis and

intelligent methods for nickel base alloy machining. CIRP Journal of Manufacturing Science and Technology, 4:327-31.

[30] D'Addona D, Segreto T, Simeone A, Teti R., 2011, ANN tool wear modelling in the machining of nickel superalloy industrial products. CIRP Journal of Manufacturing Science and Technology, 4:33-7.

[31] Diniz AE, Machado ÁR, Corrêa JG., 2016, Tool wear mechanisms in the machining of steels and stainless steels. The International Journal of Advanced Manufacturing Technology, 87:3157-68.

[32] Rimpault X, Chatelain JF, Klemberg-Sapieha JE, Balazinski M., 2017, Tool wear and surface quality assessment of CFRP trimming using fractal analyses of the cutting force signals. CIRP Journal of Manufacturing Science and Technology,16:72-80.

[33] Maier M, Zwicker R, Akbari M, Rupenyan A, Wegener K., 2019, Bayesian optimization for autonomous process set-up in turning. CIRP Journal of Manufacturing Science and Technology, 26:81-7.

[34] Bonilla Hernández AE, Beno T, Repo J, Wretland A., 2016, Integrated optimization model for cutting data selection based on maximal MRR and tool utilization in continuous machining operations. CIRP Journal of Manufacturing Science and Technology,13:46-50.

[35] Ning Y, Rahman M, Wong YS., 2001, Investigation of chip formation in high speed end milling. Journal of Materials Processing Technology, 113:360-7.

[36] Su GS, Liu ZQ., 2012, Experimental Analysis on Spherical Chips in High-Speed Machining of Hardened AerMet100. Materials Science Forum, 723:67-71.

[37] Cui X, Zhao J, Jia C, Zhou Y. Surface roughness and chip formation in high-speed face milling AISI H13 steel., 2012, The International Journal of Advanced Manufacturing Technology, 61:1-13.

[38] Amani M, Falk H, Jensen OD, Vartdal G, Aune A, Lindseth F., 2019, Color Calibration on Human Skin Images. In: Tzovaras D, Giakoumis D, Vincze M, Argyros A, editors. Computer Vision Systems. Cham: Springer International Publishing, p. 211-23.

[39] Haeghen YV, Naeyaert JMAD, Lemahieu I, Philips W., 2000, An imaging system with calibrated color image acquisition for use in dermatology. IEEE Transactions on Medical Imaging, 19:722-30.

[40] Mokrzycki W, Tatol M., 2011, Color difference Delta E - A survey. Machine Graphics and Vision, 20:383-411.

[41] Inami T., Tanimoto Y., Minami N., Yamaguchi M., Kasai K., 2015, Color stability of laboratory glass-fiber-reinforced plastics for esthetic orthodontic wires. Korean J Orthod, 45:130-5. https://dx.doi.org/10.4041%2Fkjod.2015.45.3.130.

[42] Pascale D., 2006, RGB Coordinates of the Macbeth Color Checker.

[43] Gowda CC, Mayya SG., 2014, Comparison of Back Propagation Neural Network and Genetic Algorithm Neural Network for Stream Flow Prediction. Journal of Computational Environmental Sciences.

[44] Siddique MNH, Tokhi MO., 2001, Training neural networks: backpropagation vs. genetic algorithms. IJCNN'01 International Joint Conference on Neural Networks Proceedings (Cat No01CH37222), p. 2673-8 vol.4.

[45] Djaya CRA, Sucianti N, Randy, Wulandhari LA., 2017, Hybrid Particle Swarm Optimization and Backpropagation Neural Network for Organic and Inorganic Waste Recognition. In: Silhavy R, Senkerik R, Kominkova Oplatkova Z, Prokopova Z, Silhavy P, editors. Artificial Intelligence Trends in Intelligent Systems. Cham: Springer International Publishing, p. 168-77.

Figures

Figure 1

Five-axis machine tool (EXTRON SU-85)

Figure 2

The workpiece of 2316MOD stainless steel material

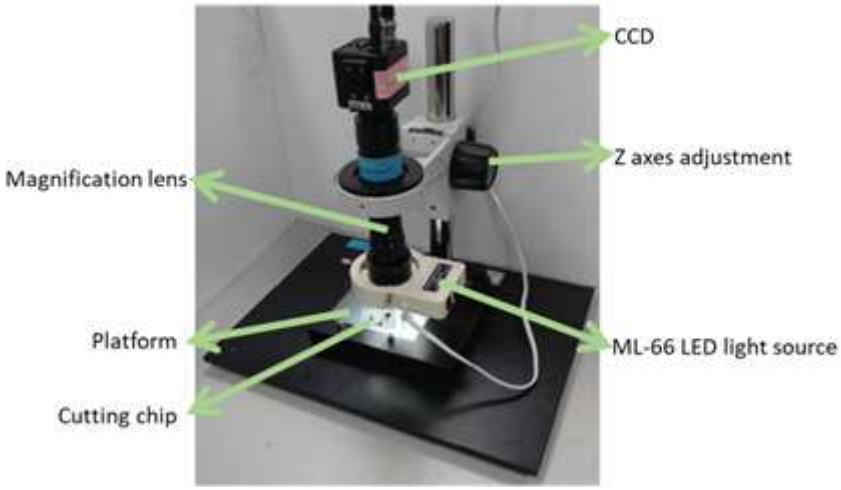

Figure 3

Wenham industrial camera equipment

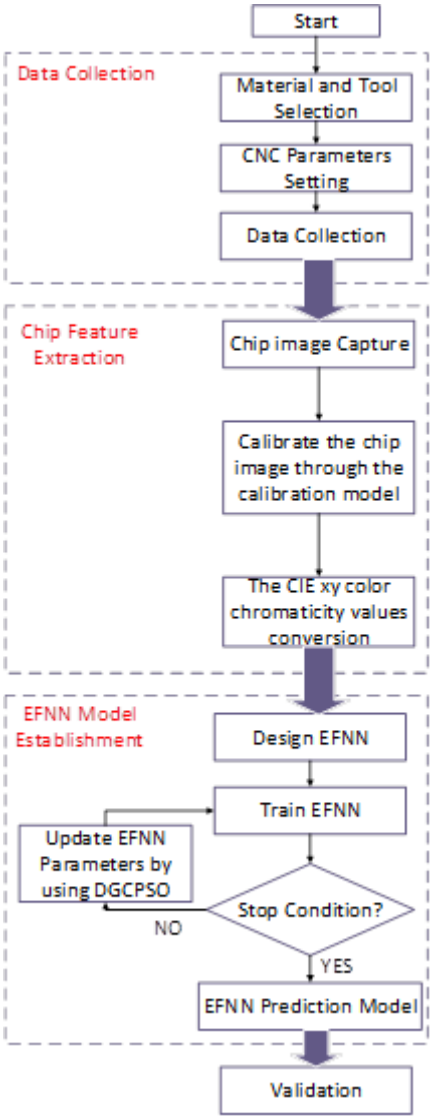

Figure 4

Flow chart of the proposed tool wear prediction framework

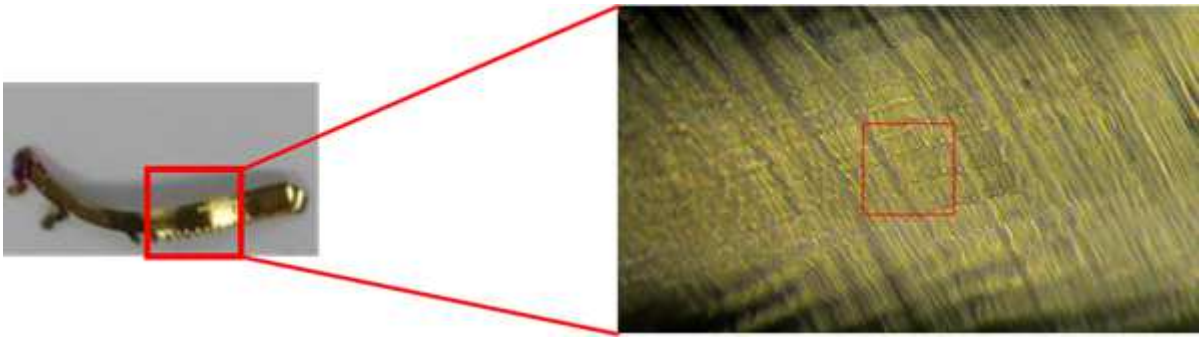

Figure 5

The chip feature image

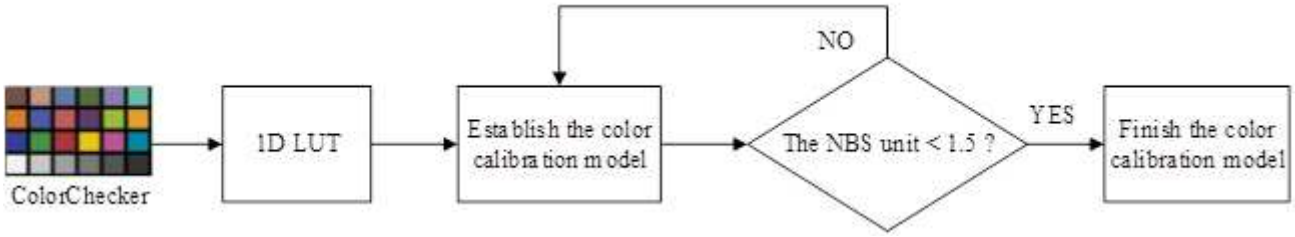

Figure 6

The flow chart of establishing color calibration model

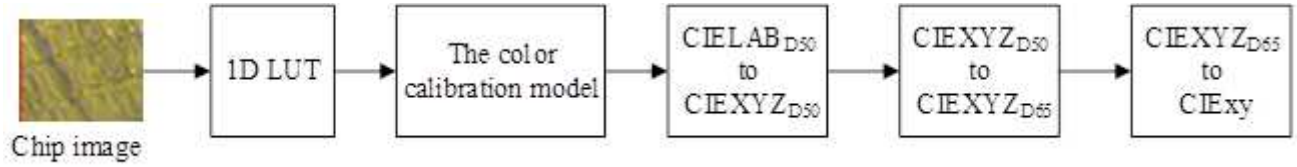

Figure 7

The flow chart of color conversion process

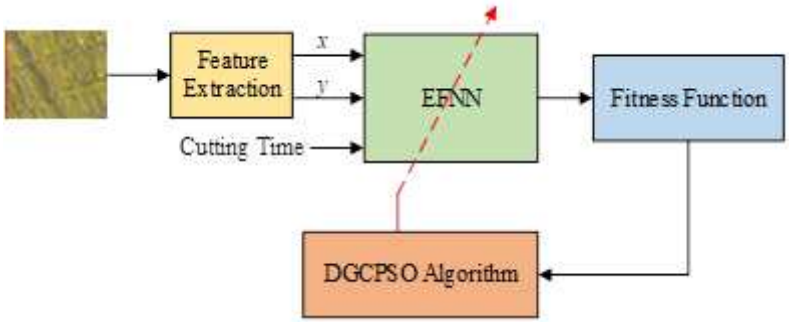

Figure 8

Tool wear prediction model architecture diagram

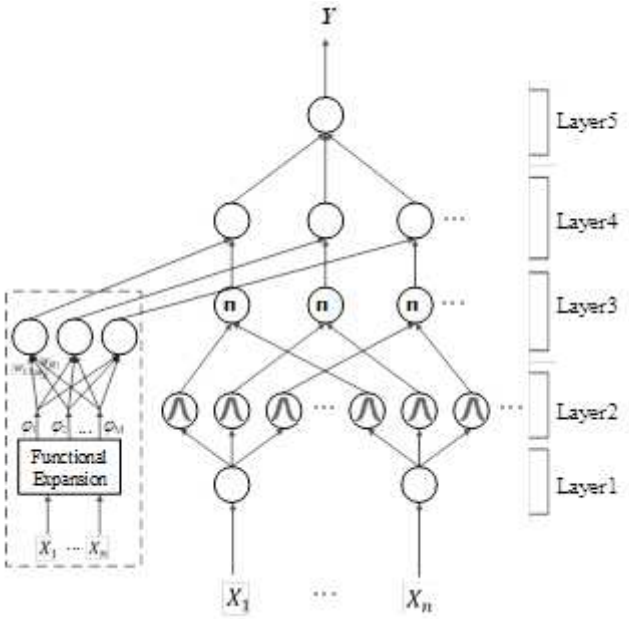

Figure 9

Evolutionary fuzzy neural network architecture

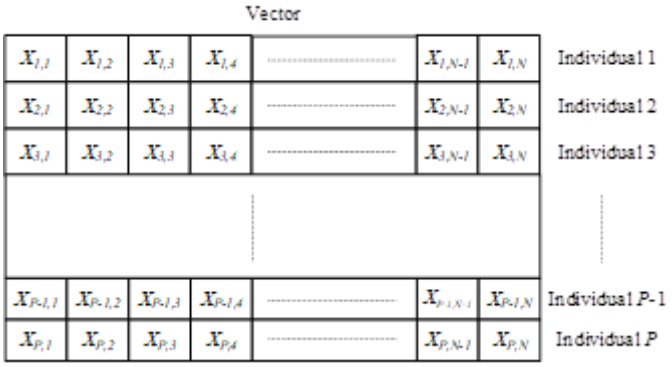

Figure 10

Traditional evolution method

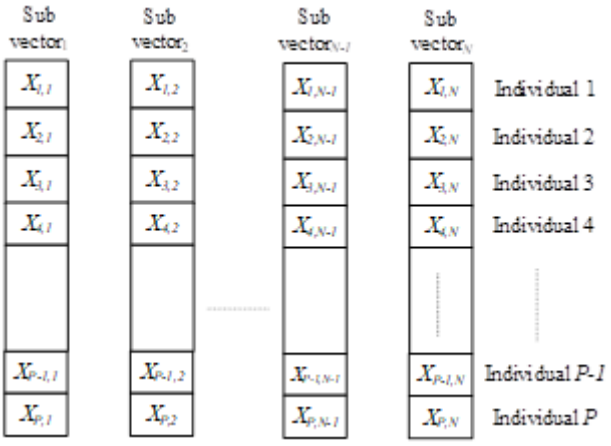

Figure 11

Cooperative evolution method

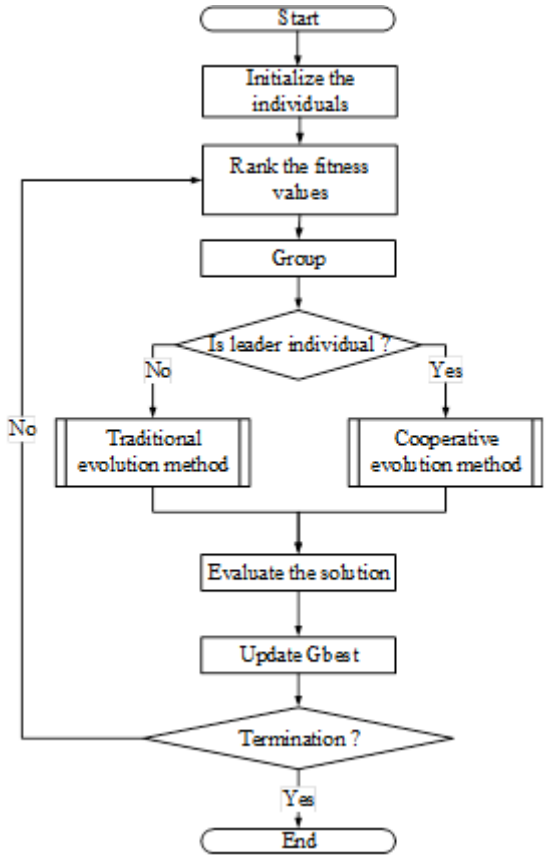

Figure 12

The flowchart of the proposed DGCPSO algorithm

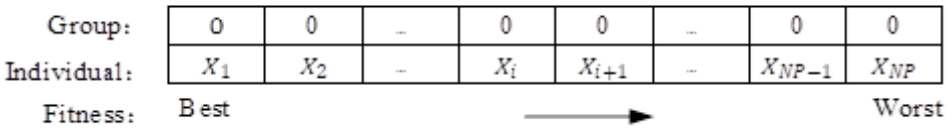

Figure 13

Ranking the order of particles

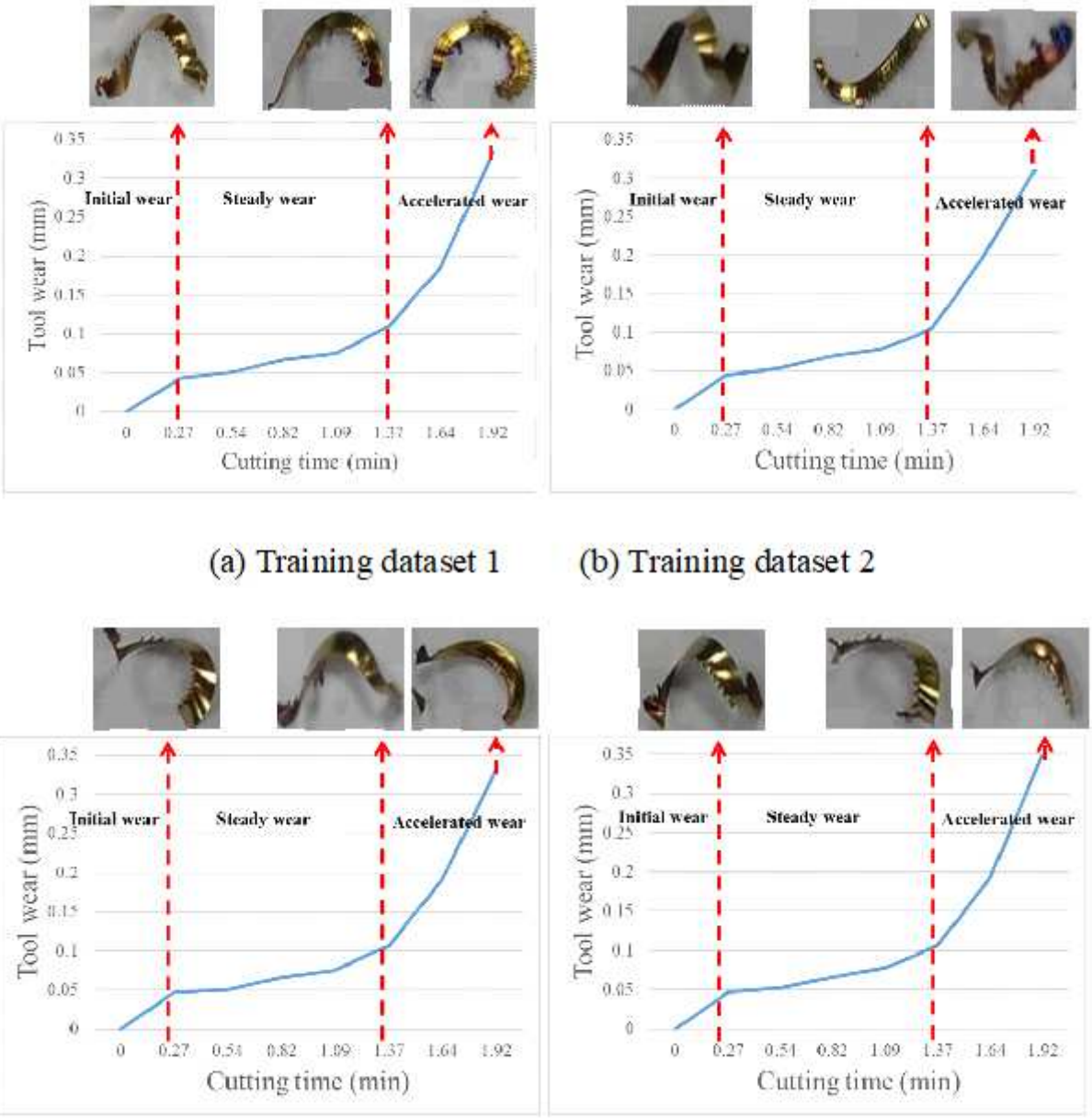

Figure 14

The datasets of cutting experiments

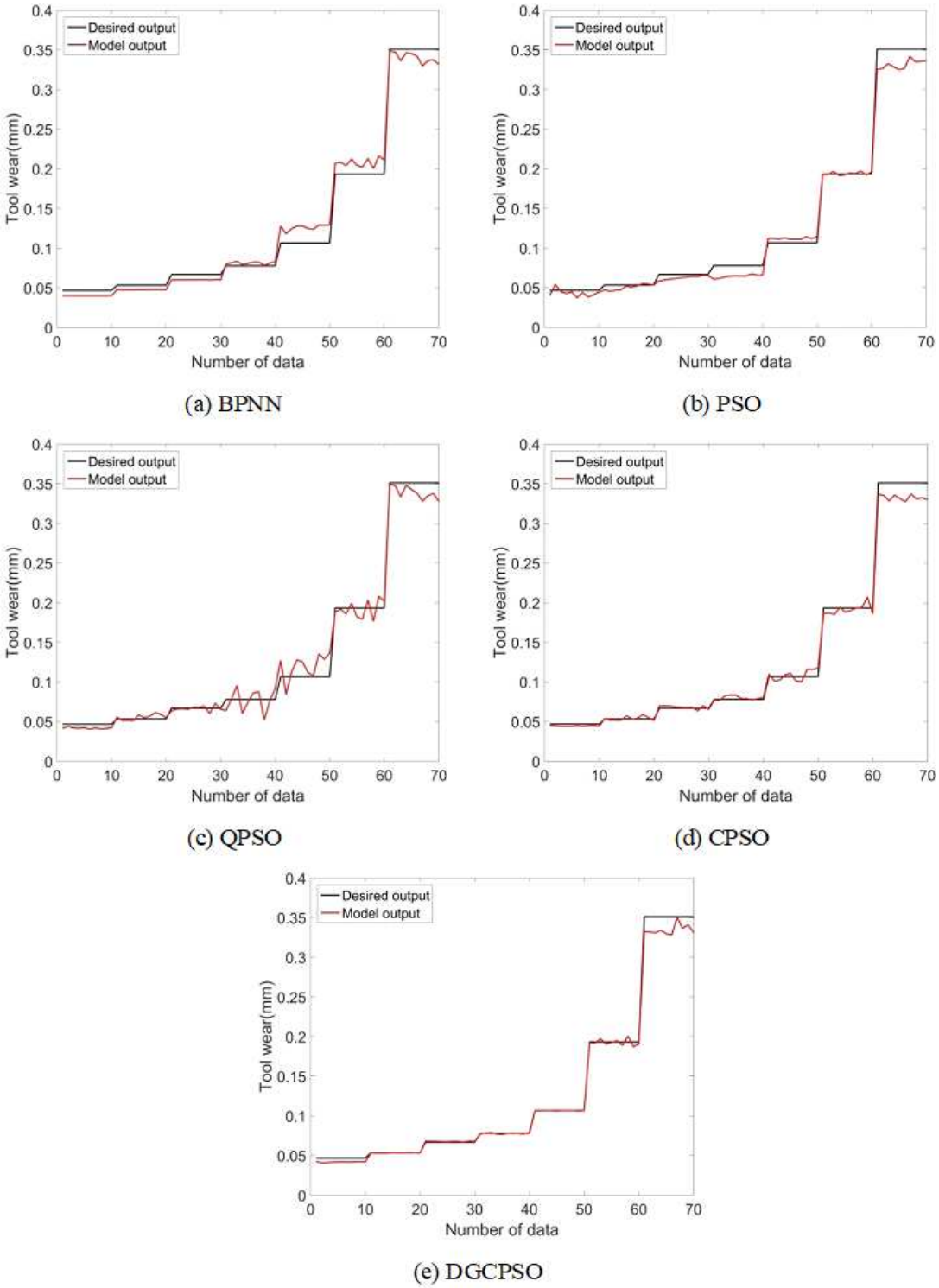

Figure 15

The prediction results of different algorithms

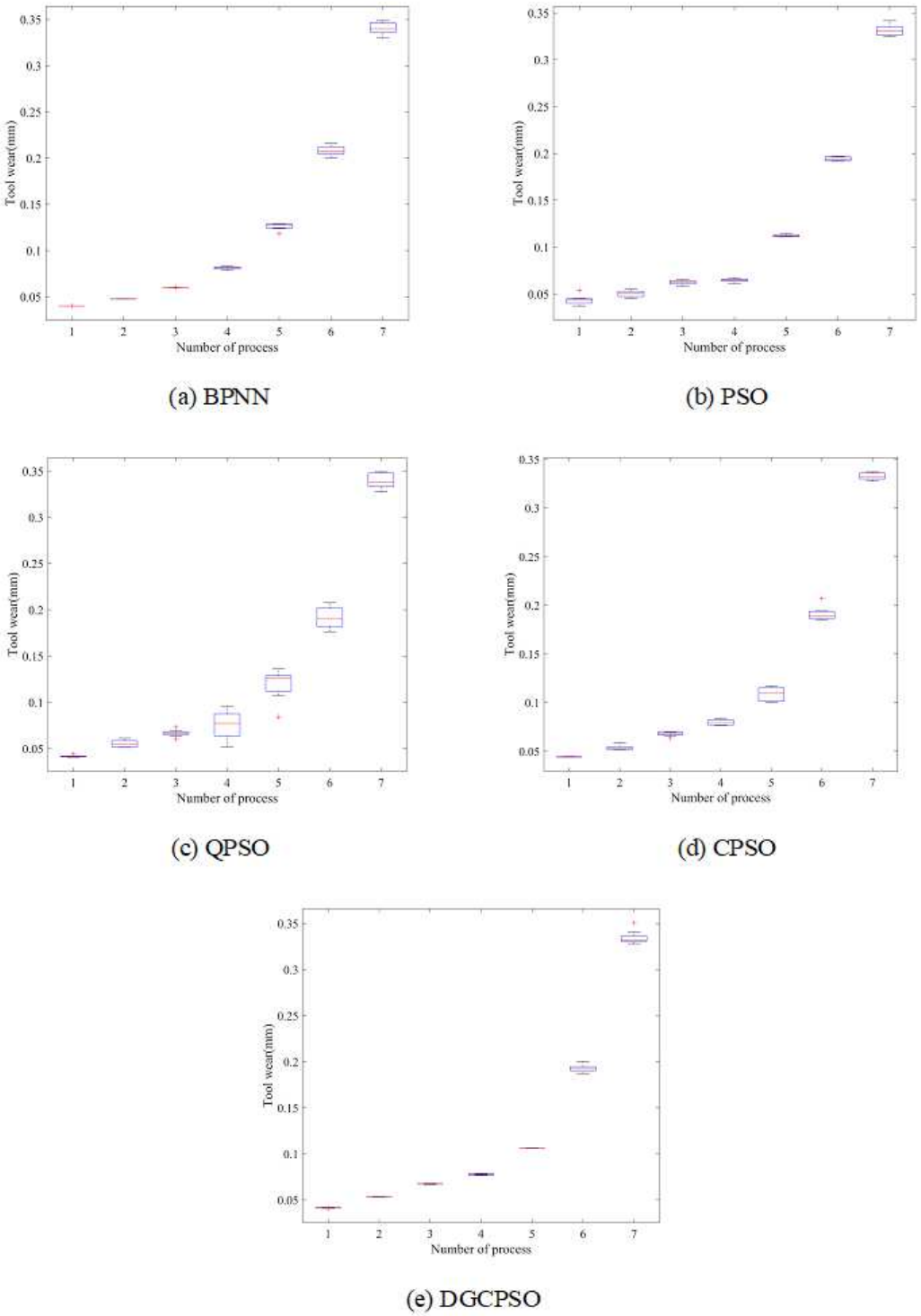

Figure 16

The boxplot of different algorithms